Steel and Composite Structures, *Vol. 18, No. 4 (2015) 925-946*
DOI: http://dx.doi.org/10.12989/scs.2015.18.4.925

Fatigue behavior of hybrid GFRP-concrete bridge decks under sagging moment

Haohui Xin [1], Yuqing Liu [*1] Jun He [2], Haifeng Fan [3] and Youyou Zhang [1]

[1] *Department of Bridge Engineering, Tongji University, Shanghai, China*
[2] *School of Civil Engineering and Architecture, Changsha University of Science & Technology, Hunan, China*
[3] *Composite Construction Laboratory CCLab, Swiss Federal Institute of Technology, BP Ecublens 1015 Lausanne, Switzerland*

(*Received November 01, 2013, Revised May 27, 2014, Accepted October 10, 2014*)

Abstract. This paper presents a new cost-effective hybrid GFRP-Concrete deck system that the GFRP panel serves as both tensile reinforcement and stay-in-place form. In order to understand the fatigue behavior of such hybrid deck, fatigue test on a full-scale specimen under sagging moment was conducted, and a series of static tests were also carried out after certain repeated loading cycles. The fatigue test results indicated that such hybrid deck has a good fatigue performance even after 3.1 million repeated loading cycles. A three-dimensional finite element model of the hybrid deck was established based on experimental work. The results from finite element analyses are in good agreement with those from the tests. In addition, flexural fatigue analysis considering the reduction in flexural stiffness and modulus under cyclic loading was carried out. The predicted flexural strength agreed well with the analytical strength from finite element simulation, and the calculated fatigue failure cycle was consistent with the result based on related S-N curve and finite element analyses. However, the flexural fatigue analytical results tended to be conservative compared to the tested results in safety side. The presented overall investigation may provide reference for the design and construction of such hybrid deck system.

Keywords: hybrid bridge deck; fatigue behavior; model test; finite element analysis; flexural fatigue analysis

1. Introduction

Nowadays, concrete and hybrid steel-concrete bridges are facing a major challenge with deterioration, which has attracted the attention of a great many researchers. It has been estimated that the average annual cost in maintenance of bridges in U.S.A during the period 1998 to 2017 could reach $5.8 billion (Kitane *et al*. 2004). Inspections have revealed that reinforcement corrosion caused by freeze-thaw cycles and various chemicals is one of the main reasons for this deterioration (Berg *et al*. 2006, Klowak *et al*. 2006). According to an investigation done by Chinese government in 2012, about 15% of existing bridges in China are suffering from this problem. Among various bridge components, bridge decks are directly subjected to the repeated

*Corresponding author, Ph.D., Professor, E-mail: yql@tongji.edu.cn

http://www.techno-press.org/?journal=scs&subpage=8 ISSN: 1229-9367 (Print), 1598-6233 (Online)

moving wheel loads. Thus, they are especially vulnerable to be deteriorated under fatigue loads.

Due to high strength, light weight and non-corrodible nature, Fiber Reinforced Polymer (FRP) composites are one of the promising alternative materials to solve the above-mentioned problems. Researchers have attempted various applications of FRP in bridge deck systems. Three major types of bridge decks using FRP composites are concrete bridge decks reinforced with FRP bars or FRP grids (Bank *et al*. 2006, El-Ragaby *et al*. 2007a, b), all FRP composite bridge decks (Bakis *et al*. 2002, Kumar *et al*. 2004, Wan *et al*. 2005, Keller and Gürtle 2005, Jeong *et al*. 2007, Lee *et al*. 2007, Park *et al*. 2007, Liu *et al*. 2008) and hybrid FRP-concrete bridge decks (Hillman and Murray 1990, Bakeri and Sunder 1990, Van Erp *et al*. 2005, Keller *et al*. 2007, Alnahhal and Aref 2008, Alnahhal *et al*. 2008, Schaumann *et al*. 2008).

Compared with concrete bridge decks reinforced with FRP bars or grids, all FRP composite bridge decks are much lighter and more convenient to construct. To date, various types of all FRP composite bridge decks have been proposed like Superdeck (Bakis *et al*. 2002), Strongwell (Kumar *et al*. 2004), DuraSpan (Wan *et al*. 2005), and Asset (Keller and Gürtle 2005) system. These decks usually consist of uniform modules with different configurations such as trapezoidal, rectangular, square, or triangular shapes. However, all FRP composite bridge decks also highlight some weakness like high initial costs and low stiffness. In order to overcome these drawbacks, an innovative concept of hybrid FRP-concrete panel structure was proposed (Bakeri and Sunder 1990, Hillman and Murray 1990). Concrete is used to substitute FRP composites in the compression zone. Furthermore, FRP profiles in the hybrid structures are usually used as stay-in-place (SIP) forms, which may reduce the construction time and labor cost significantly.

Various kinds of hybrid FRP-concrete bridge deck systems have been designed and studied in the past several decades. Van Erp *et al*. (2005), Kitane *et al*. (2004), Alnahhal and and Aref (2008) and Alnahhal *et al*. (2008b) proposed a similar type of hybrid FRP-concrete decks consisting of FRP hollow profiles in the tension zone and a layer of concrete in the compression zone. Another type of hybrid bridge deck was investigated by Keller *et al*. (2007), Schaumann *et al*. (2008) and Hanus *et al*. (2008), consisting of FRP sheet with T-upstands or grids as SIP forms and concrete cast on them. Chen *et al*. (2009) proposed a hybrid FRP-concrete bridge deck system consisting of U-shaped FRP beams and reinforced concrete slab in the compression zone. These two components were connected using shear connectors. He *et al*. (2012) proposed a novel cost-effective hybrid GFRP and concrete deck, and conducted sand filling test and static flexural load tests. Experimental results indicated that the stiffness and strength of GFRP plate under construction loading meets the requirements of relative codes. Static test of GFRP bridge deck filled with foam was carried out by Zi *et al*. (2008), and the results showed that filled foam improved the transverse direction behaviors. The flexural behavior of the GFRP–concrete hybrid solution in continuous structural elements was studied by Correia *et al*. (2009). Cho *et al*. (2010) carried out static test and fatigue test of innovative mixed shear connection system to investigate the behavioral characteristics of shear connection between FRP and concrete, showing the static and fatigue composition performance was enhanced. The failure mode, fatigue performance were studied and the ultimate and service load were determined based on experiments including specimens of deck panels, positive moment capacity beams experiment, negative moment capacity beams, and the fatigue beam (Dieter *et al*. 2002). Full scale deck slab specimens were tested under simulated wheel design load to investigate the static response, ultimate capacity and failure mechanics (Ringelstetter *et al*. 2006).

Based on previous research works reviewed above, a hybrid glass fiber reinforced polymer (GFRP)-concrete bridge deck is proposed (He *et al*. 2012). It consists of corrugated GFRP bottom

plates with ribs, GFRP reinforcements, and concrete. In addition, the corrugated pultruded GFRP plate with T-upstands also acts as a permanent formwork. In this study, fatigue test on a full-scale specimen under sagging moment was conducted, and a series of static tests were also carried out after certain repeated loading cycles. During fatigue test, the deflection, strains of concrete and GFRP plate, cracking as well as slip at interface were measured to investigate long-term performance. A three-dimensional finite element model of hybrid deck was established based on experimental works, and finite element analysis (FEA) results were compared with the test results to verify the proposed model. In addition, flexural fatigue analysis considering the reduction in flexural stiffness and modulus under cyclic loading was conducted. The analyzed results were compared to the tested ones in terms of strength and stiffness. All the results of experimental study, numerical analyses and theoretical study for such hybrid deck in this paper may provide reference for the design and construction of such type deck system.

2. Experimental program

2.1 Test specimen

As is shown in Fig. 1(a), a full-scale specimen (3.0 × 1.0 × 0.2 m) was fabricated by setting reinforcements and casting concrete on the bottom GFRP plate assembled from two unit modules through bolt connections. Corrugated GFRP plate with T-upstands and cross-section of the deck are shown in Figs. 1(b) and (c) respectively. Diameter and center-to-center spacing of the holes on the perfobond GFRP ribs were chosen as 50 mm and 150 mm (Fig. 1(d)). 4800TEX alkali-free glass fibers were used for GFRP pultruded profiles, and the mechanical properties of GFRP pultruded profiles were measured through a series of material tests. The measured material properties of GFRP profile are shown in Table 1. Material properties of GFRP reinforced bars used in this study were provided by the manufacturer. Tensile strength of GFRP bars with the diameter of 16 mm used for distribution-bars and cross-bars was 655 MPa, while tensile strength of GFRP bars with the diameter of 19 mm for compression bars was 620 MPa. Elastic modulus of both type GFRP bars was between 35 to 41 GPa. Three cube specimens and four prism specimens were made and moist cured alongside the test specimens. The cube specimens (150 × 150 × 150 mm) were used to investigate the compressive strength of concrete at 28 days. Axial compressive strength and elastic modulus of concrete were determined from the prism specimens (100 × 100 × 300 mm). Compressive strength (f_{cu}), axial compressive strength (f_c), and elastic modulus (E_c) of the concrete were 43.3 MPa, 37.5 MPa, and 34.5 GPa respectively.

In order to improve the bonding condition of GFRP plate, epoxy adhesive was applied on the top surface of GFRP bottom plate and on the flanges of T-shaped perfobond ribs. Before the adhesive cured, clean quartz sands (2 to 4 mm in diameters) were spread over the surface.

Table 1 Material properties of GFRP profile

Properties	Direction	Strength (MPa)	Elastic modulus (GPa)
Tensile	Longitudinal	492	32
Compressive	Longitudinal	847	75
	Transverse	187	22
Flexural	Longitudinal	590	22

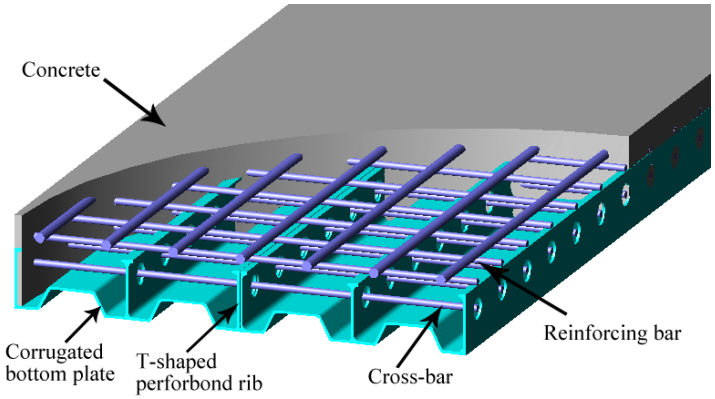

(a) Hybrid bridge deck

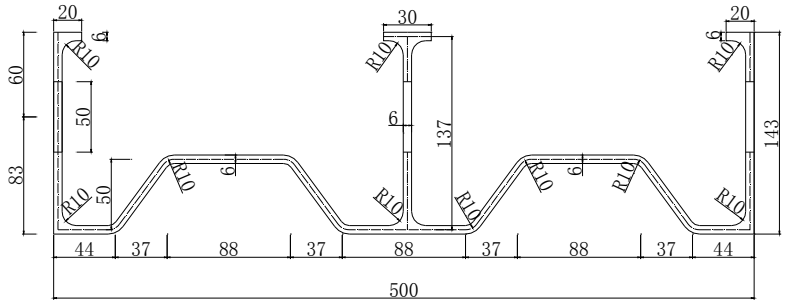

(b) Corrugated plate with perfobond ribs

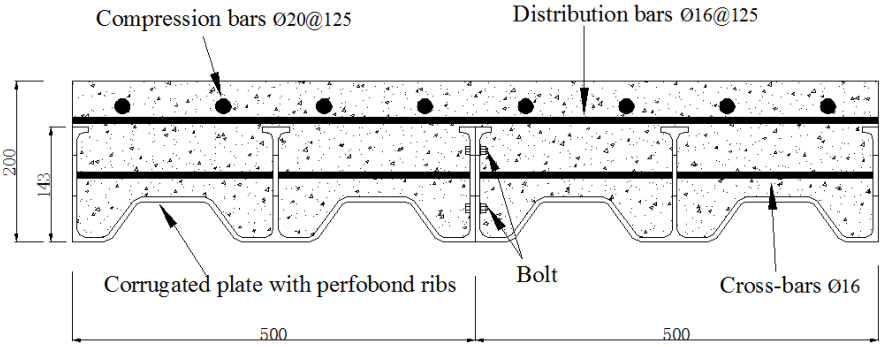

(c) Cross-section

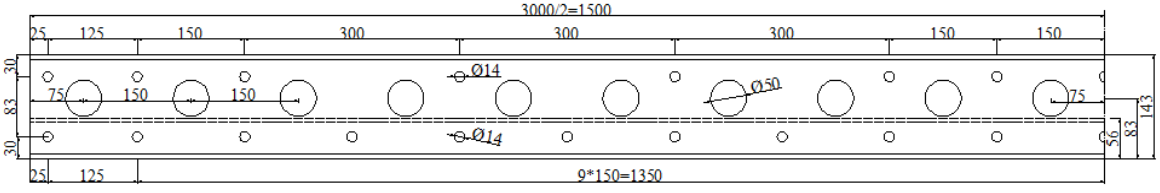

(d) Side view of corrugated plate

Fig. 1 Proposed hybrid FRP-concrete bridge deck (mm)

2.2 Test setup and instrumentation layout

Experimental setup and instrumentation layout are shown in Fig. 2. The specimen were simply supported on rollers with a span of 2.5 m and subjected to four-point bending load. In order to protect the bottom surface of specimens, elastomeric bearing pads and steel plates were placed between the specimen and rollers. The fatigue loading was applied by a PMS-500 fatigue testing machine with loading capacity of 500 kN and frequency of 3.5 Hz. LVDTs 1 and 2 were installed under the deck to acquire the deflection at the mid-span. LVDTs 3 to 5 were used to measure the relative slip between concrete and GFRP bottom plate. The stain gages were installed to measure the strain at bottom GFRP plate, top concrete and side GFRP plate, which were denoted as B, T and S respectively. Besides, in order to investigate the structural performance of the deck specimen during the fatigue test, dynamic deflection at the mid-span was measured after every 0.05 million cycles at a frequency of 100 Hz. Load, deflection and strain results were continuously recorded during the tests using a high-speed data acquisition system (DH3816).

2.3 Loading procedure

The design load of such deck was 127.4 kN. The maximum applied load was determined to be 200 kN (1.5 × 127.4 kN) to keep same deflection by considering the difference between single point loading at mid-span and two points loading at quarter-span. The minimum applied load was chosen to be 100 kN, depending on dead load. The specimen was subjected to 3.1 million cycles of constant amplitude loading (100 to 200 kN) at a frequency of 3.5 Hz. After 0.01, 0.05, 0.1, 0.5, 1, 2 and 2.5 million cycles, fatigue test was stopped temporary. The specimen was then subjected to a static load up to 200 kN to investigate the structural performance after different fatigue loading cycles.

3. Results and discussion

Deterioration of the deck specimen due to cyclic loadings would be obvious from the increase of deflections and strains. These parameters were measured during the monotonic loading steps

(a) Experimental set-up

Fig. 2 Experimental setup and instrumentation layout of fatigue test

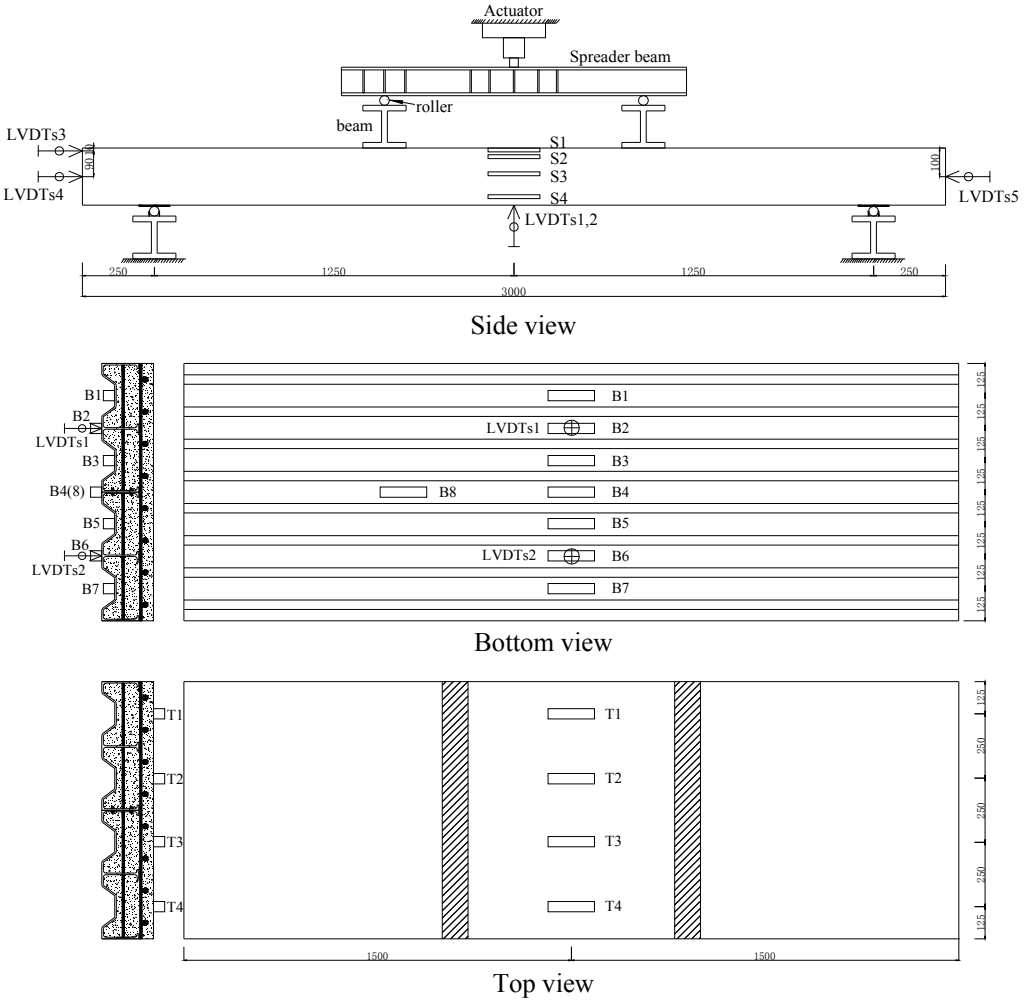

(b) Specimen and instrumentation layout (mm)

Fig. 2 Continued

carried out at the end of certain fatigue loading cycles. In addition, cracking initiation and development during fatigue loading stages were well marked on the concrete surface.

3.1 Crack development

Before fatigue test, a static test (0 cycles) was performed on the hybrid deck, no cracks were observed. Development of fatigue cracks during the whole test is shown in Fig. 3. The fatigue cracks initiated from the interface between the concrete and the flange of mid T-shaped ribs at the end of deck after 0.03 million cycles. Then, these cracks progressed up to the top surface and developed slowly towards the mid-span with the increased number of loading cycles. Besides, the width of all the cracks was very small, this kind of longitudinal cracks were might due to the corrugated configuration of the bottom plate.

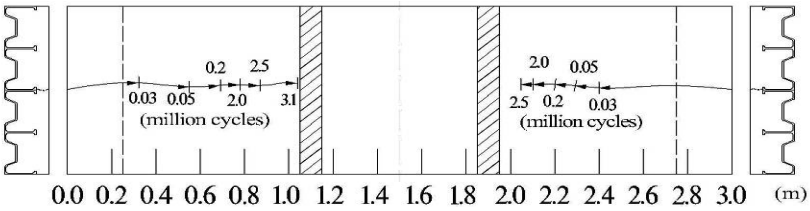

Fig. 3 Development of fatigue cracks during the fatigue test

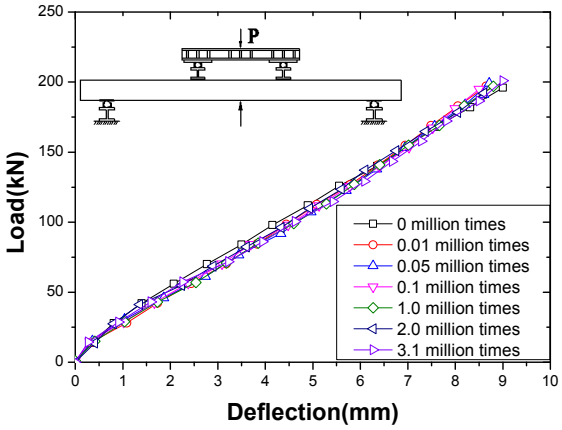

Fig. 4 Load-deflection curve at mid-span

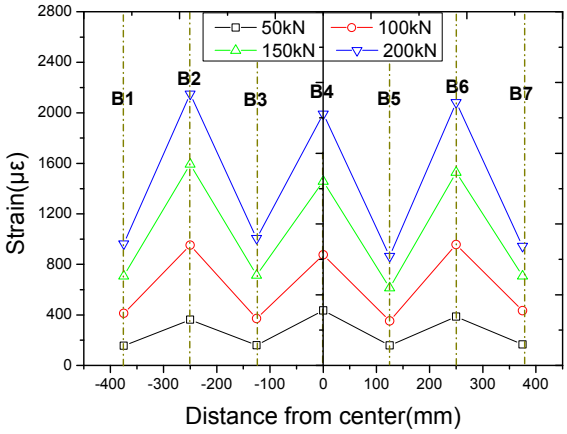

Fig. 5 Distribution of FRP strains at mid-span section

3.2 Load-deflection relationship

Fig. 4 shows the static load-deflection behavior for the specimen recorded at the end of certain fatigue loading cycles. No apparent stiffness degradation was observed during the test. In addition, the load-deflection response of the specimen was almost linear up to the maximum load of 200 kN. The deck system is still in elastic stage without stiffness degradation even after 3 million repeated loading cycles.

3.3 Strain variations

Static test was carried out before fatigue test, and the distribution of GFRP strains at mid-span section was presented in Fig. 5, the GFRP strains change along transverse direction. The distribution of GFRP strains was in accord with the shape of GFRP plate, with maximum strain at crest and minimum strain at trough.

The strain variations at the center of bottom GFRP plate were shown in Fig. 6. It indicated that the tensile strain of the bottom GFRP plate increased almost linearly with applied load. And the strains increased gradually with the repeated loading cycles, due to cracks in the bottom concrete appeared after first static test, which leading to stiffness degradation of this component. Thus, load was redistributed and the load resisted by bottom plate was increased.

Distribution of strains at side face of the specimen is shown in Fig. 7. The results showed that the strain is in a linear relation along height at 0 million times loading in elastic stage which

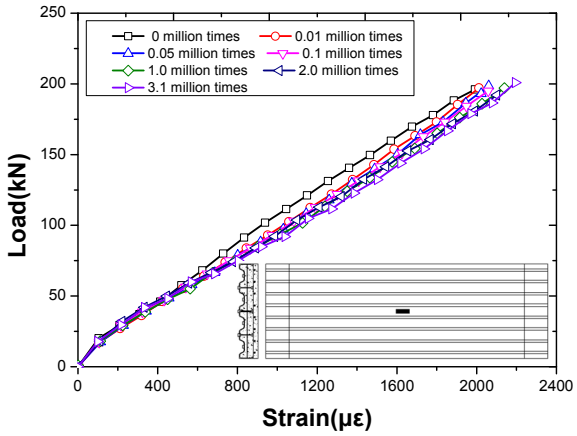

Fig. 6 FRP strain variations at the center of the bottom FRP plate

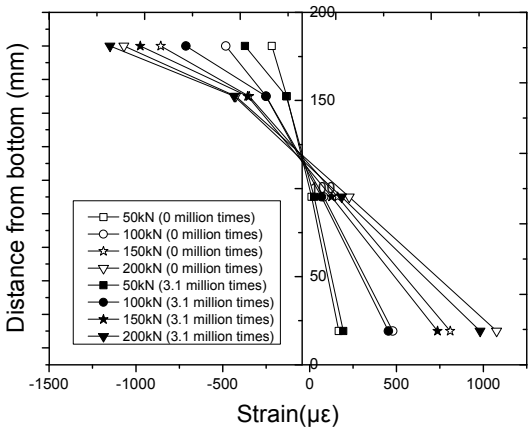

Fig. 7 Distribution of strains at side face of the specimen

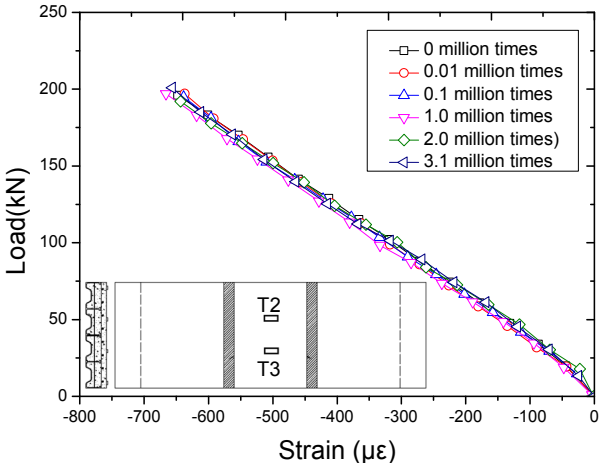

Fig. 8 Concrete strain variations at the top surface in mid-span

accords with plane section assumption. Strain deviation appeared after 3.1 million times loading cycle. It indicated that the ratio of stress resisted by GFRP and concrete changed when concrete cracks occurred.

The compressive concrete strains (mean value of T2 and T3) at the top surface during the test were shown in Fig. 8. It was shown that the compressive strains of the concrete did not increase during the whole fatigue test.

3.4 Dynamic deflections

The maximum dynamic deflection, minimum dynamic deflection, the difference between maximum and minimum dynamic deflections (D-Value) and remnant deflections are summarized in Figs. 9 and 10.The results showed both maximum and minimum dynamic deflections increased steadily as the increase of loading cycles. In addition, D-Value almost remained constant, which

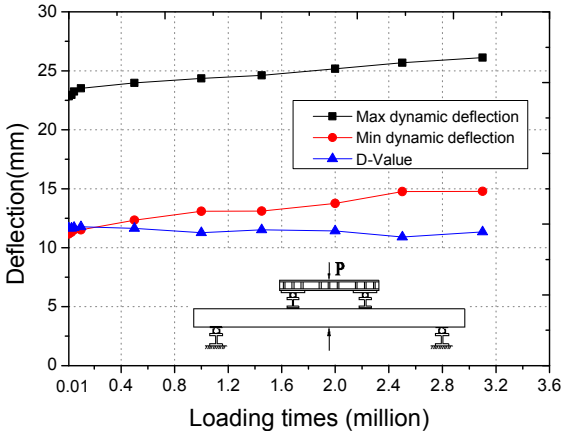

Fig. 9 Dynamic deflections at mid-span

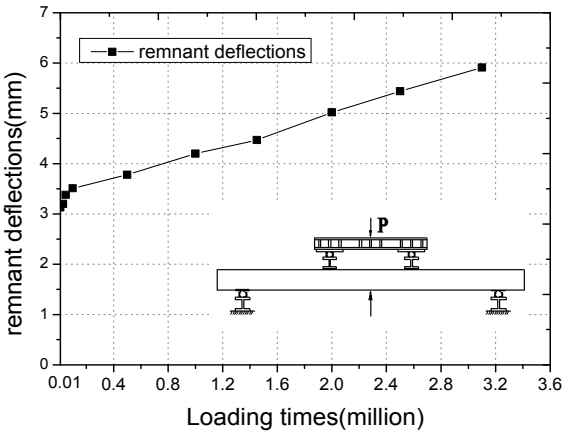

Fig. 10 Remnant deflections at mid-span

showed that the stiffness of deck specimen had no significant degradation. Besides, residual deflection after certain fatigue loading cycles increased slightly as shown in Fig. 10. It was indicated that the damage accumulated steadily throughout the fatigue test. Fatigue cracks occurred in the test had steadily induced the deterioration of concrete, but it had little effect on the stiffness of whole structure.

4. Finite element analysisd

4.1 Finite element model

The numerical model of hybrid GFRP-Concrete bridge deck was established by using finite element method and commercial software ABAQUS (ABAQUS 2005), as shown in Fig. 11. Solid element (C3D8R) was used to simulate bottom GFRP plate, and the orthogonal anisotropy properties were realized by setting different parameters in different directions. The material properties of GFRP plate in finite element model was adopted from material test results, as shown in Table 1. Besides, the GFRP reinforcing bars through the holes were also simulated by solid elements (C3D8R), but the longitudinal and distribution bars were simulated by beam elements (T3D2). The modulus of elasticity and tensile strength of GFRP bars were 35 GPa and 620 MPa respectively.

The concrete was also represented by solid element (C3D8R).The uniaxial compressive stress-strain relationship was obtained based on Eqs. (1)~(3) according to Eurocode4 (1994). The tensile stress-strain relationship was adopted to be linear before reaching the ultimate tensile stress. Because the stress-strain relationship would introduce unreasonable mesh sensitivity into results if there are not enough reinforcements in significant regions of the model (ABAQUS 2005), the stress-displacement relationship, which can be acquired based on Eq.(4)~Eq.(7), was adopted to simulate the post-failure behavior (CEB-FIP 2010). The elastic property of concrete in finite element model was adopted from material test results as above mentioned. The concrete plastic-damage model was adopted considering concrete cracking and concrete crush. The plastic property was defined as the difference between total property calculated by Eqs. (1)~(7) and

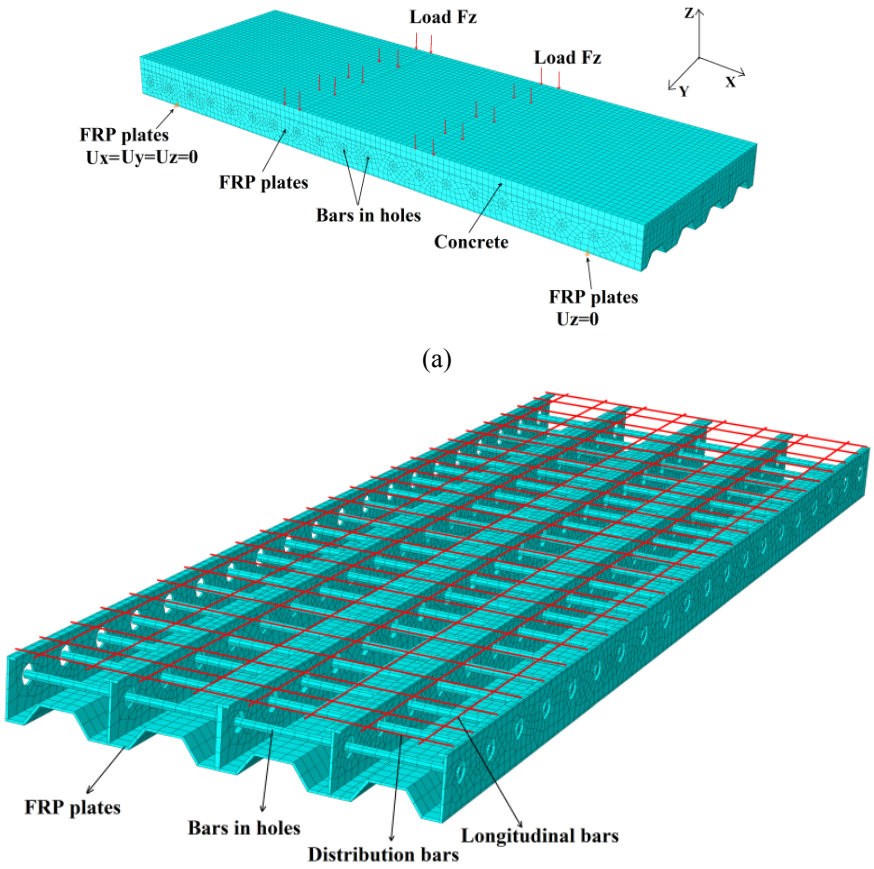

Fig. 11 FE Model of hybrid deck

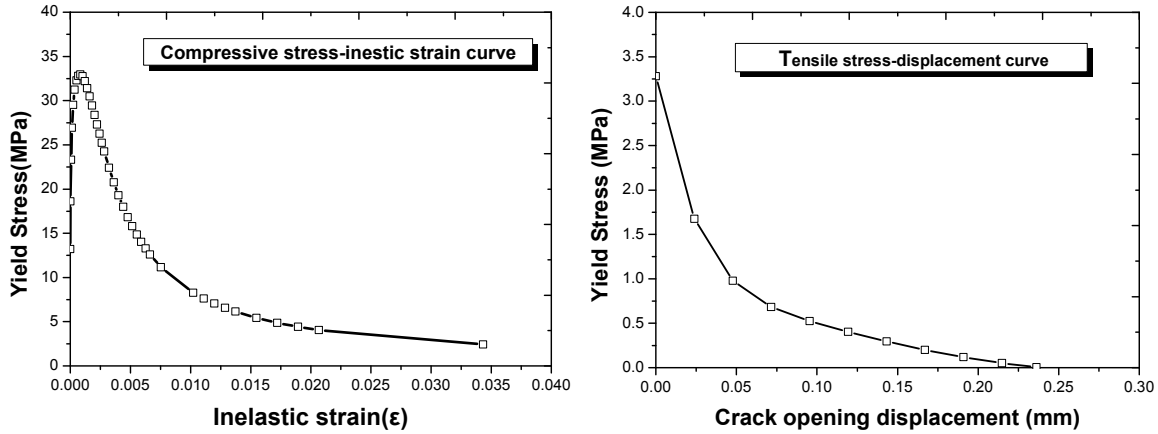

(a) Compressive stress-strain curve (b) Tensile stress-strain curve

Fig. 12 Concrete plastic-damage constitutive relation

Table 2 The parameters of plastic-damage model

Dilatation angle	Flow potential of skewness	f_{b0}/f_{c0}	k	coefficient of viscosity
30	0.1	1.16	0.6667	0.0005

elastic property (ABAQUS 2005). The concrete plastic-damage constitutive relation in ABAQUS was shown in Fig. 12. And the parameters of plastic-damage model were summarized in Table 2. In which, the expression of "f_{b0}/f_{c0}" is the ratio of initial equibiaxial compressive yield stress to initial uniaxial compressive yield stress, the letter 'k' represents the ratio of the second stress invariant on the tensile meridian to that on the compressive meridian at initial yield for any given value of the pressure invariante.

$$\frac{\sigma_c}{f_{cm}} = \frac{k\eta - \eta^2}{1 + (k-2)\eta} \tag{1}$$

$$\eta = \frac{\varepsilon_c}{\varepsilon_{c1}} \tag{2}$$

$$k = 1.05E_{cm}\frac{\varepsilon_{c1}}{f_{cm}} \tag{3}$$

$$\frac{\sigma_t}{f_t} = f(w) - \frac{w}{w_c}f(w_c) \tag{4}$$

$$f(w) = \left[1 + \left(\frac{c_1 w}{w_c}\right)^3\right] e^{\left(-\frac{c_2 w}{w_c}\right)} \tag{5}$$

$$G_f = 73 f_{cm}^{0.18} \tag{6}$$

$$w_c = \frac{5.14 G_f}{f_t} \tag{7}$$

where, σ_c is the compressive stress, ε_c is the compressive strain, σ_t is the tensile stress, ε_{c1} is the peak strain, f_{cm} is the ultimate compressive strength, E_{cm} is the elastic modulus, f_t is ultimate tensile stress, w is crack opening displacement, w_c is crack opening displacement at which stress can no longer transferred, $c_1 = 3.0$, $c_2 = 6.93$ for normal density concrete. G_f is the energy required to open a unit area of crack.

The bonding condition between concrete and longitudinal (or distribution) bars were assumed to be perfectly constrained. The interactions between FRP plates and concrete, between bars in holes and related concrete were simulated by hard contact in the normal direction and penalty in the tangential direction in order to consider slip between concrete and FRP. The friction coefficient used in the tangential direction is generally between 0 and 1, and parametric study was carried out to investigate the influence of friction coefficient.

According to actual support condition of test, as shown in Fig. 11(a), all the degrees of freedoms were restricted on one end of the hybrid deck, and vertical displacement (UZ) was restricted on the other end. Pressure was applied on the corresponding top concrete surface to simulate test loading.

4.2 Numerical results

4.2.1 Comparison of test and finite element analysis results

The mid-span deflection, stress at the top of concrete surface, and stress at the center of bottom GFRP plate (0 cycles) were observed, and compared to numerical results with different friction coefficient used in the tangential direction. The compared load-deflection curve, load-stress curves are shown in Fig. 13. It was shown that the stiffness increased with friction coefficient from 0.1 to

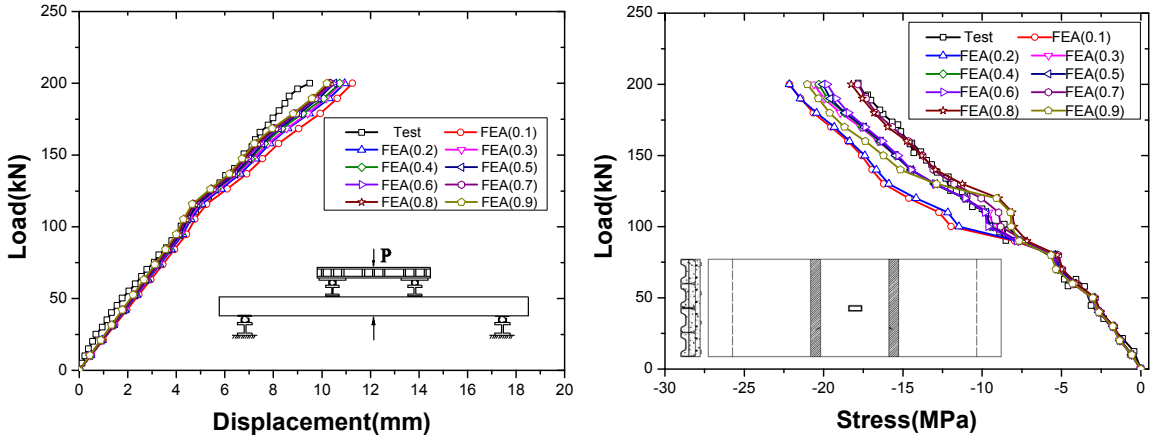

(a) Comprison of mid-span deflection (b) Comprision of concrete stress

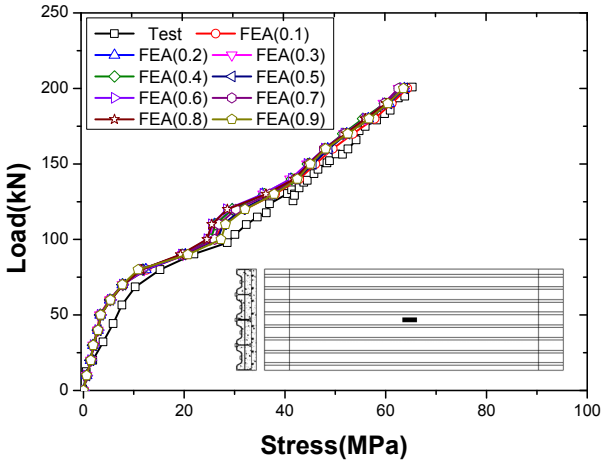

(c) Comparison of GFRP stress

Fig. 13 Comparison of test and simulation results

0.9, but the increasing stiffness amplitude is relatively small. The test results of concrete stress are consistent with the FEA results with friction coefficient between 0.7 and 0.9. Friction coefficient has less influence on FRP stress. Thus, the results from finite element analyses with friction coefficient from 0.7 to 0.9 are in good agreement with those from the tests. The friction coefficient with 0.7 is recommended in this paper considering safety.

4.2.2 Stress distribution

The stress distributions of top concrete at mid-span were obtained from FE analysis, as depicted in Fig. 14. It can be found that the stress amplitude of top concrete surface distributed uniformly, the maximum compressive stress and stress amplitude were 20.08 MPa and 11.56 MPa respectively. The tensile strain distributions of bottom concrete at mid-span were shown in Fig. 15, the maximum tensile strain was 2891.27 $\mu\varepsilon$, and the strains fluctuated due to the distance change from bottom to neutral axis. The stress distribution of GFRP plate at mid-span was shown in

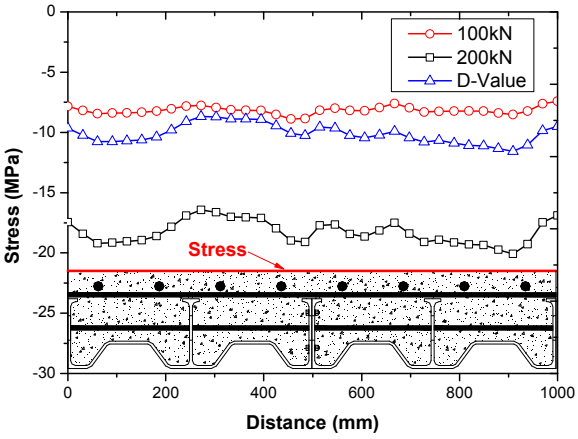

Fig. 14 The stress distribution of top concrete at mid-span

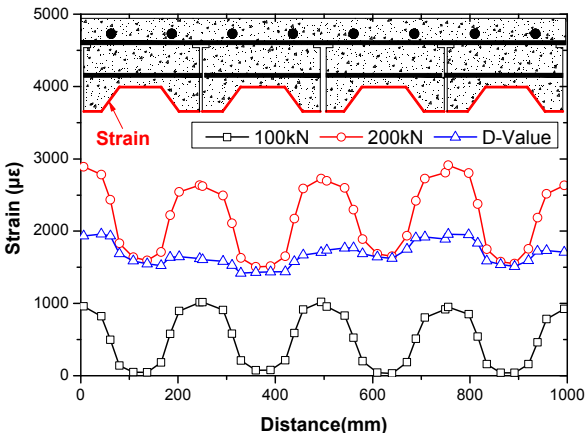

Fig. 15 The strain distribution of bottom concrete at mid-span

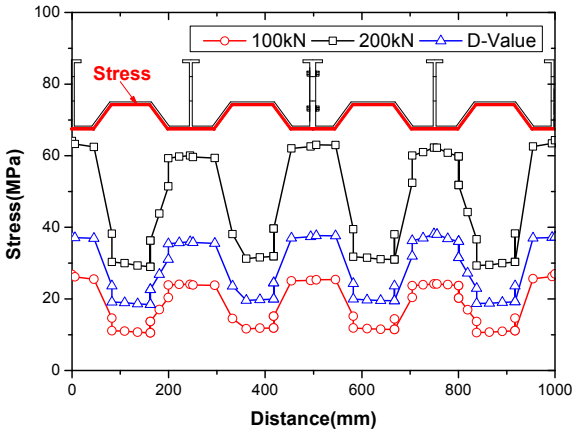

Fig. 16 The stress amplitude of FRP plate at mid-span

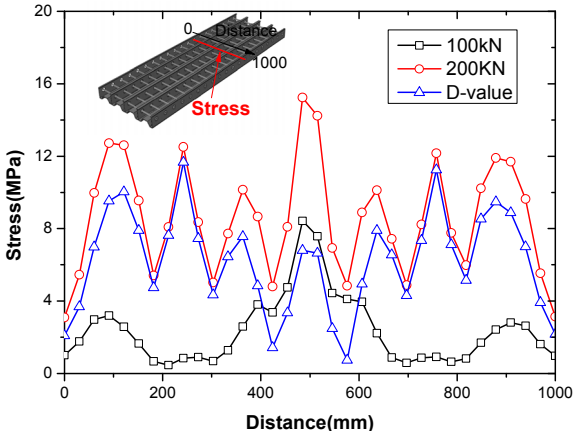

Fig. 17 The stress amplitude of penetrating rebars in holes

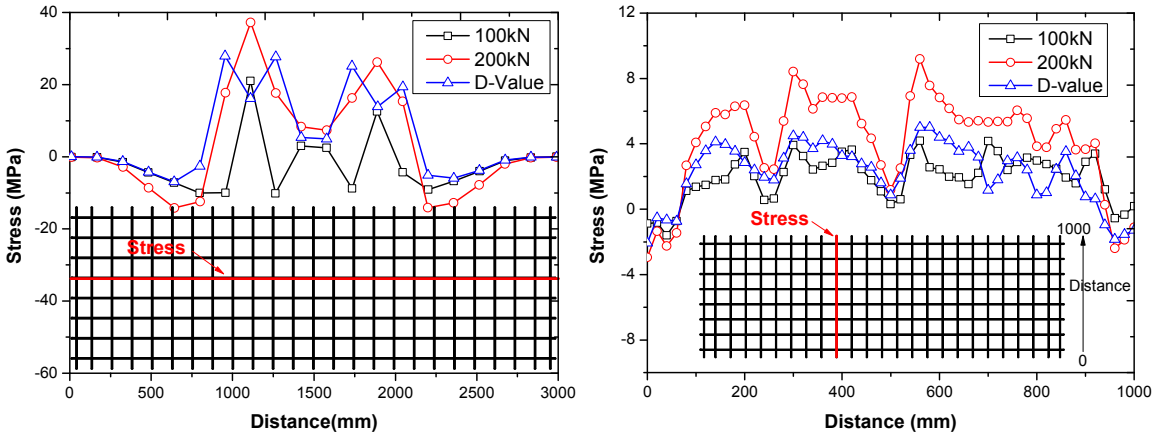

(a) Stress distribution of longitudinal bar (b) Stress distribution of transverse bars

Fig. 18 The stress distribution of reinforcing bars

Fig. 16, it was indicated that the stress of GFRP plate were fluctuated up and down, but opposite to corrugated plate shape. The maximum stress (64.1 MPa) appeared at trough of GFRP plate. The rebar in holes with maximum stress amplitude was selected and the stress distribution was also demonstrated in Fig. 17. The stress also changed up and down along transverse distance, and the maximum stress (15.2 MPa) and maximum stress amplitude (6.2 MPa) both occurred at the center of hybrid deck. The stress distribution of reinforcing bars with maximum stress amplitude was depicted in Fig. 18. The maximum stress of longitudinal bar appeared near the loading point. The stress of transverse bar distributed non-uniformly, and the maximum stress occurred at a quarter of total length.

4.2.3 Fatigue life prediction

FRP composites have a better fatigue resistance than other materials such as steel and concrete, due to FRP composites are commonly made of layers of unidirectional or angled fiber/matrix composites, and cracks in the matrix does not easily propagated (Cheng 2011). For little contribution to the strength, the fatigue degradation in the E-glass layers was neglected (Sendeckyj *et al*. 1990, Cheng and Karbhari 2006). Thus, the strength and stiffness degradation in the FRP composites were insignificant and were assumed to be negligible during fatigue analysis (Cheng 2011). The fatigue failure cycles of such hybrid deck was mainly due to concrete deterioration. The relationship between stress levels (S) and loading times (N) for determining the fatigue strength of normally vibrated concrete was adopted, and the relationship as Eq. (8) was recommended to represent the conventional S-N diagram (Cheng and Karbhari 2006). Based on former studies (Oh 1986, Goel *et al*. 2012), the coefficients (A and B) of fiber reinforced concrete beams was determined to be 1.0401 and -0.0575 respectively. Thus, the fatigue failure cycles (5.88×10^8) was obtained, which indicated such hybrid deck has a superior fatigue performance.

$$S = \frac{f_{\max}}{f_r} = A + B\log_{10}(N) \tag{8}$$

where $f_{\max}$ is maximum fatigue stress, f_r is static flexural strength, A and B are experimental

coefficients.

5. Static and fatigue flexural analysis

5.1 Theoretical static flexural analysis

Some assumptions were adopted to simplify the flexural analysis in this study, as following: (1) perfect bonding between GFRP and concrete based on test results; (2) contribution of the tensile stress from T-upstands is negligible; (3) the average strain along the cross-section depth obeys the plain section assumption at elastic stage; (4) contribution of the cracked concrete is ignored, (5) the GFRP forms remain elastic behavior; (6) the final failure is governed by concrete crushing or rupture of GFRP in tension.

The calculation diagram was depicted in Figs. 19~22 when the deck is under elastic stage before concrete cracking, concrete cracking, concrete in the compression zone under elastic stage and concrete in the compression zone under elastic-plastic phase respectively. The bending curvature (φ) when concrete under elastic stage, initial concrete cracked and concrete in the compression zone under elastic stage are described in Eq. (9), when concrete in the compression zone under elastic-plastic phase is summarized in Eq. (10) according to geometric relation.

$$\phi = \frac{\varepsilon_t}{h-x} = \frac{\varepsilon_c}{x} = \frac{\varepsilon_{fi}}{h_i - x} = \frac{\varepsilon_r}{x-a} \tag{9}$$

$$\phi = \frac{\varepsilon_c}{x} = \frac{\varepsilon_{fi}}{h_i - x} = \frac{\varepsilon_r}{x-a} = \frac{\varepsilon_c'}{x-y_c} \tag{10}$$

where, h_i is the distance from centroid to the top surface, a is the distance from the location of GFRP bars to the top surface, x is the height of neutral axis, ε_{fi} *is* the tensile strain of GFRP plate; ε_{ti} *is* the tensile strain of concrete, ε_r *is* the compressive strain of GFRP reinforcing bars, ε_{ci} *is* the compressive strain of concrete.

The equilibrium condition of forces can be derived as the following equation for each stage. Thus, the neutral axis depth (x) can be obtained.

$$F_{\text{con}}^c + F_r^c = \sum_{i=1}^{3} F_{fi}^t + F_{\text{con}}^t \tag{11}$$

where, F_{con}^c is compressive resultant force of concrete, F_{con}^t is tensile resultant force of concrete, F_r^c is compressive resultant force of rebar, F_{fi}^t is tensile resultant force of FRP profile.

The moment can be calculated as follows

$$M = \sum_{i=1}^{3} F_{fi}^t (h_i - a) + F_{\text{con}}^c h_{cc} + F_{\text{con}}^t h_{ct} \tag{12}$$

where, h_{cc} is the distance from the point of F_{con}^t to the centroid of rebar; h_{ct} is the distance from the point of F_{con}^t to the centroid of rebar.

The comparisons of the theoretical, FE and static test results were summarized in Table 3.

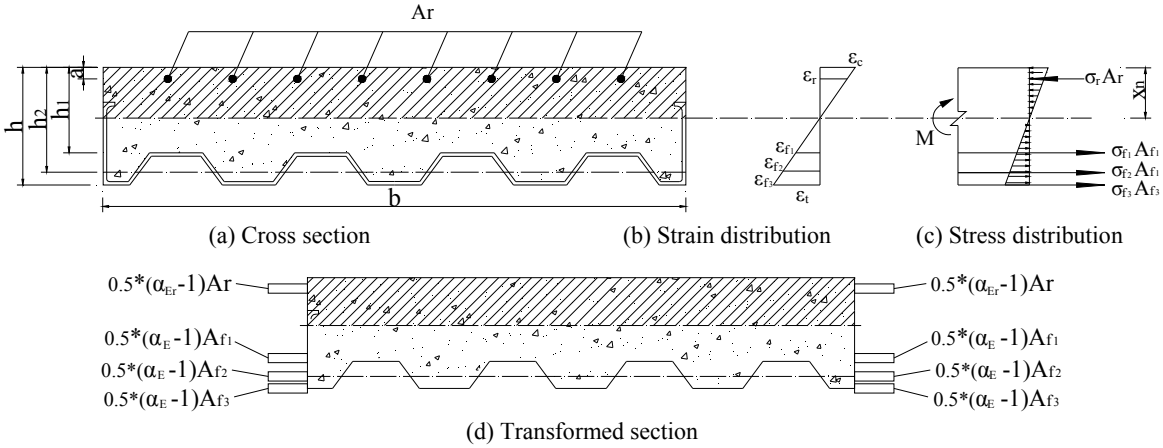

(a) Cross section (b) Strain distribution (c) Stress distribution

(d) Transformed section

Fig. 19 Calculation diagram under elastic stage

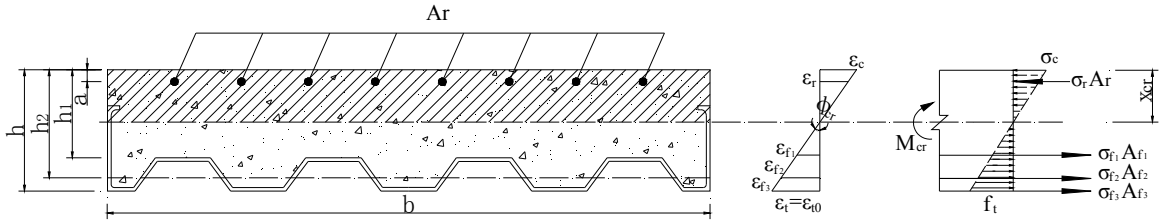

(a) Cross section (b) Strain distribution (c) Stress distribution

Fig. 20 Calculation diagram when concrete cracking

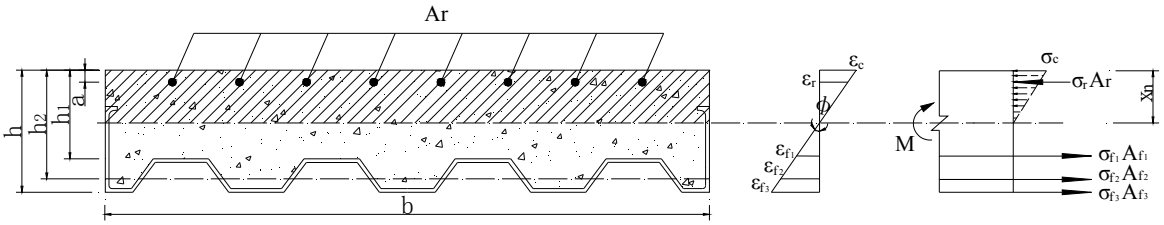

(a) Cross section (b) Strain distribution (c) Stress distribution

Fig. 21 Calculation diagram when concrete in the compression zone under elastic stage

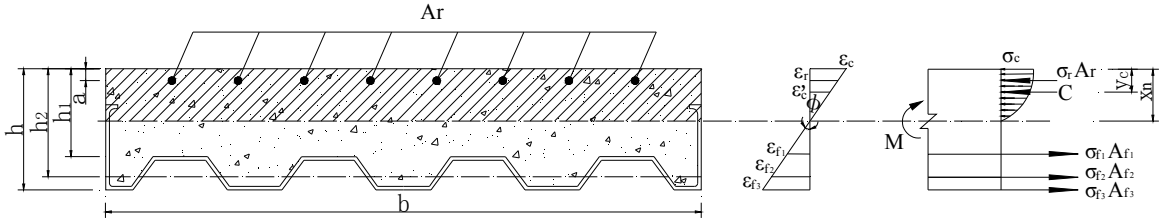

(a) Cross section (b) Strain distribution (c) Stress distribution

Fig. 22 Calculation diagram when concrete in the compression zone under elastic-plastic phase

Table 3 Comparison of theoretical, FE and static test results

Stage	Load (kN)	Mid-span concrete strain ($\mu\varepsilon$)			Mid-span FRP strain ($\mu\varepsilon$)		
		Theoretical	FE	Test	Theoretical	FE	Test
(1) before concrete cracking	20	-39.7	-33.7	-30.4	51.3	52.08	58.1
(2) when concrete cracking	35.6	-94.1	-80.1	-84.6	124.0	101.7	130.0
(3) the concrete in the compressive zone under elastic-plastic phase	100	-284.3	-257.6	-276.5	979.3	884.76	893.7
	200	-588.8	-524.2	-521.7	2510.1	2171.76	2177.1

These results show that theoretical results can predict the strain of concrete and GFRP plate for hybrid GFRP-concrete deck.

5.2 Theoretical fatigue flexural analysis

From fatigue loading test, it showed that the strength and stiffness degradation of GFRP composites were insignificant and could be assumed negligible during fatigue analysis for such hybrid deck. The strength and stiffness degradation were mainly due to concrete damage. The cyclic creep strain (Cheng 2011) of concrete could be obtained by Eqs. (13)~(15), and the cycle dependent secant modulus of elasticity for concrete in compression after N fatigue cycles can be calculated by Eq. (16).

$$\varepsilon_{c,N_1} = 129\sigma_m t^{1/3} + 17.8\sigma_m \Delta N^{1/3} \tag{13}$$

$$\sigma_m = \frac{(\sigma_{\max} + \sigma_{\min})}{(2f_c)} \tag{14}$$

$$\Delta = \frac{(\sigma_{\max} - \sigma_{\min})}{(f_c)} \tag{15}$$

$$E_N = \frac{\sigma_{\max}}{\frac{\sigma_{\max}}{E} + \varepsilon_{c,N_1}} \tag{16}$$

where, $\varepsilon_{c,N}$ is the cyclic creep strain; σ_m is the mean stress ratio; t is the time computed in hours; Δ is the stress range; $\sigma_{\max}$ is the maximum compressive stress; $\sigma_{\min}$ is the minimum compressive stress; N is the number of cycles; f_c is the nominal compressive strength of concrete; E is modulus of elasticity; E_N is the cycle-dependent secant modulus of elasticity for concrete in compression.

5.2.1 Stress distribution

The concrete in the compressive zone (at load level of 200 kN) was under elastic-plastic stage based on test results. Thus, the cycle-dependent neutral axis depth ($x_{n,N}$) can be obtained by Eq. (17) based on modified concrete strain (ε_c) and modified elasticity modulus of concrete (E_c) in the neutral axis depth equation calculated by Eq. (12). Then, the stress distribution of concrete after

certain fatigue cycles (N) can be obtained from the relation of cycle-dependent neutral axis depth and modified concrete strain in Eq. (10).

$$x_n = \frac{2}{b(8\varepsilon_0 - 3\varepsilon_{c,N})}\left(-3\varepsilon_0\omega_N + \sqrt{9\varepsilon_0^2\xi_N + 18\varepsilon_0^2\Delta_N + 18\varepsilon_0^2\Gamma_N + (24b\varepsilon_0^2 - 9b\varepsilon_{c,N}\varepsilon_0)\beta_N}\right)$$

$$\omega_N = \alpha_{E,N}\omega_1 + \alpha_{Er,N}\omega_2, \qquad \xi_N = \alpha_{E,N}^2\xi_1 + \alpha_{Er,N}^2\xi_2, \tag{17}$$

$$\Delta_N = \alpha_{E,N}^2\Delta_1 + \alpha_{E,N}\alpha_{Er,N}\Delta_2, \quad \beta_N = \alpha_{E,N}\beta_1 + \alpha_{Er,N}\beta_2, \quad \Gamma_N = \alpha_{E,N}^2\omega_1 + \alpha_{Er,N}\omega_2$$

$$\varepsilon_{c,N} = \varepsilon_c + \varepsilon_{c,N_1}, \quad \alpha_{E,N} = \frac{E_f}{E_N}, \quad \alpha_{E,N} = \frac{E_r}{E_N} \tag{18}$$

$$\phi_{n,N} = \frac{\varepsilon_c}{x_{n,N}} = \frac{\varepsilon_{fi}}{h_i - x_{n,N}} = \frac{\varepsilon_r}{x_{n,N} - a} \tag{19}$$

where, $\varepsilon_{c,N}$ is the cycle-dependent concrete strain; $\alpha_{E,N}$ is the cycle-dependent ratio of E_f to E_N, $\alpha_{r,N}$ is the cycle-dependent ratio of E_r to E_N.

5.2.2 Deflection distribution

The deflection under repeated loading cycles was obtained according to conventional beam theory, considering cycle-dependent moment of inertia and elasticity modulus (N). The deflection of the hybrid deck can be calculated as follows

$$d = \frac{\phi(load, span)}{E_N I_{EN}} \tag{20}$$

where, φ(load, span) is a function related to the applied load, the span length, loading and boundary conditions.

The moment of inertia for cracked cross-section ($I_{cr,N}$) including moment of inertia of GFRP, rebars and concrete, which can be calculated as follows

$$I_{cr,N} = I_{con,N} + I_{FRP,N} + I_{rebar,N} \tag{21}$$

The cycle-dependent effective moment of inertia ($I_{e,N}$) provides a transition between the gross moment of inertia (I_g) and cracked moment of inertia ($I_{cr,N}$) after a number of cycles (N). This effective moment of inertia can be obtained by Eq. (22) based on ACI (Cheng 2011, ACI 1999).

$$I_{e,N} = I_{cr,N} + \left(\frac{M_{cr,N}}{M_a}\right)^3 \left(I_g - I_{cr,N}\right) \tag{22}$$

5.3 Comparisons of theoretical and tested results

As shown in Fig. 23, the comparisons of tested and calculated stress at the top surface of

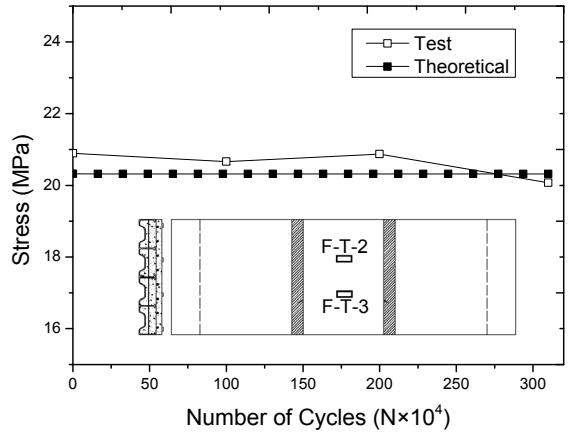

(a) Average concrete stress at top surface in mid-span

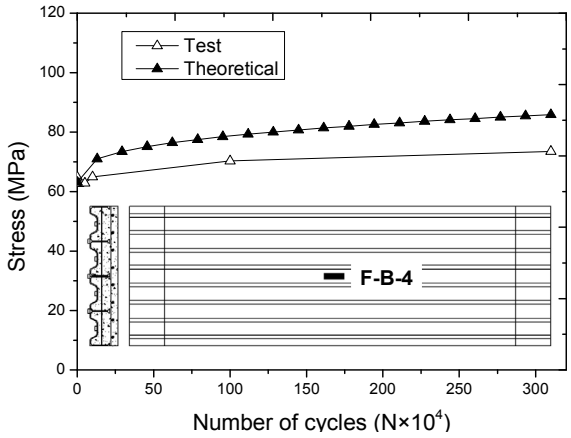

(b) Stress at the center of the bottom FRP plate

Fig. 23 Comparison of tested and theoretical calculation stress

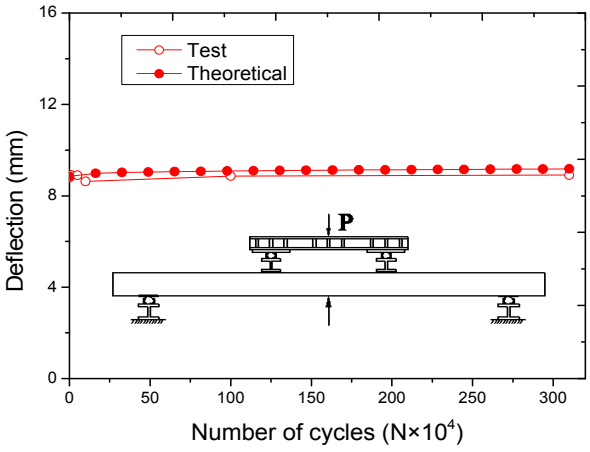

Fig. 24 Comparison of tested and theoretical calculation deflection

concrete, and stress at the center of the bottom GFRP plate in mid-span were figured out. The results showed that the concrete stress at the top surface in mid-span from theoretical calculation agreed well with those from tests. The tensile stress of the bottom GFRP plate at mid-span from theoretical calculation was slightly larger than those from tests, and the maximum difference was within 10%, which might be because of ignoring the concrete and T-upstands contribution in the tensile zone. The comparison of tested and calculated deflection at mid-span was shown in Fig. 24. The predicted mid-span deflection was slightly larger than tested one, and the maximum difference was within 5%. The reason for this difference was same as that for the error in tensile stress of GFRP plate mentioned above. If the fatigue cycles increased to 5.86×10^8, the cycle-dependent concrete strain increased to ultimate strain (0.0033) resulting in concrete crush, which had a good agreement with the fatigue failure cycle analysis (5.88×10^8) based on related S-N curve (Eq. (8)).

6. Conclusions

The fatigue behavior of a new type of hybrid GFRP-concrete bridge deck system has been experimentally investigated through model test. On the basis of experimental results, finite element model and theoretical method were applied to evaluate the fatigue performance. The following conclusions can be drawn from the present study:

(1) The fatigue test results indicated that such hybrid deck has a good fatigue performance even after 3.1 million cycles. No apparent stiffness and strength degradation of hybrid deck system occurred as the increase of repeated cycles. Only micro cracks initiated at the interface between concrete and GFRP plate, indicating a good composite performance. These micro cracks were might due to the corrugated configuration of the bottom plate and can be ignored for durability in terms of such corrosion resistant steel-free deck.
(2) A three-dimensional finite element model of hybrid deck was established on the basis of experimental specimen. The results of strength and stiffness from finite element analyses are in good agreement with those from the tests. Fatigue failure cycle was evaluated based on related S-N curve and finite element analyses results.
(3) Flexural fatigue analysis taking into account the reduction in flexural stiffness and elasticity modulus under cyclic loading was conducted. The results of predicted flexural strength agreed well with those from the finite element analysis, and the calculated fatigue failure cycle was consistent with the result on the basis of related S-N curve and finite element analyses. However, the flexural fatigue analysis results tended to be conservative compared to the tested results in safety side.

Acknowledgments

The authors gratefully acknowledge the financial support provided by the Science and technology project (No. 2013318822370) of Ministry of Transport of the people's republic of China.

References

ABAQUS Inc. (2005), ABAQUS Theory Manual [M].
ACI Committee (1999), Building code requirements for structural concrete, American Concrete Institute; pp.

96-101.
Alnahhal, W. and Aref, A. (2008), "Structural performance of hybrid fiber reinforced polymer–concrete bridge superstructure systems", *Compos. Struct.*, **84**(4), 319-336.
Alnahhal, W., Aref, A. and Alampalli, S. (2008), "Composite behavior of hybrid FRP-concrete bridge decks on steel girders",*Compos. Struct.*, **84**(1), 29-43.
Bakeri, P.A. and Sunder, S.S. (1990), "Concepts for hybrid FRP bridge deck systems", In: *Serviceability and Durability of Construction Materials*; *Proceedings of the Materials Engineering Congress*, Denver, CO, USA, August.
Bakis, C.E., Bank, L.C., Brown, V.L., Cosenza, E., Davalos, J.F., Lesko, J.J., Machida, A., Rizkalla, S.H. and Triantafillou, T.C. (2002), "Fiber-reinforced polymer composites for concstruction – State-of-art review", *J. Compos. Constr.*, **6**(2), 73-88.
Bank, L.C., Oliva, M.G., Russell, J.S., Jacobson, D.A., Conachen, M., Nelson, B. and McMonigal, D. (2006), "Double-layer prefabricated FRP grids for rapid bridge deck construction: case study", *J. Compos. Constr.*, **10**(3), 204-212.
Berg, A.C., Bank, L.C., Oliva, M.G. and Russell, J.S. (2006), "Construction and cost analysis of an FRP reinforced concrete bridge deck", *Constr. Build. Mater.*, **20**(8), 515-526.
Chen, Y., Ziehl, P.H. and Harrison, K.W. (2009), "Experimental characterization and optimization of hybrid FRP-RC bridge superstructure system", *Chinese J. Bridge Eng.*, **14**(1), 45-54. [In Chinese]
Cheng, L. and Karbhari, V.M. (2006), "Fatigue behavior of a steel-free FRP-concrete modular bridge deck system", *J. Bridge Eng. ASCE*, **11**(4), 474-488.
Cheng, L. (2011), "Flexural fatigue analysis of a CFRP form reinforced concrete bridge deck", *Compos. Struct.*, **93**(11), 2895-2902
Cho, K., Park, S.Y., Kim, S.T., Cho, J.R. and Kim, B.S. (2010), "Shear Connection System and Performance Evaluation of FRP-concrete Composite Deck", *KSCE J. Civil Eng.*, **14**(6), 855-865.
Correia, J.R., Branco, F.A. and Ferreira, J.G. (2009), "Flexural behaviour of multi-span GFRP–concrete hybrid beams", *Eng. Struct.*, **31**(7),1369-1381.
Dieter, D.A., Dietsche, J.S., Bank, L.C., Oliva, M.G. and Russell, J.S. (2002), "Concrete bridge decks constructed with fiber-reinforced polymer stay-in-place forms and grid reinforcing", *Transport. Res. Rec.: J. Transport. Res. Board*, **1814**, 219-226.
El-Ragaby, A., El-Salakawy, E. and Benmokrane, B. (2007a), "Fatigue life evaluation of concrete bridge deck slabs reinforced with glass FRP composite bars", *J. Compos. Constr.*, **11**(3), 258-268.
El-Ragaby, A., El-Salakawy, E. and Benmokrane, B. (2007b), "Fatigue analysis of concrete bridge deck slabs reinforced with E-glass-vinyl ester FRP reinforcing bars", *Compos. Part B*, **38**(5-6), 703-711.
Eurocode 4 (1994), Design of composite steel and concrete structures; Part 1-1: General rules and rules for buildings.
Goel, S., Singh, S.P. and Singh, P. (2012), "Flexural fatigue strength and failure probability of self compacting fibre reinforced concrete beams", *Eng. Struct.*, **40**, 131-140.
Hanus, J.P., Bank, L.C. and Oliva, M.G. (2008), "Combined loading of a bridge deck reinforced with a structural FRP stay-in-place form", *Constr. Build. Mater.*, **23**(4), 1605-1619.
He, J., Liu, Y.Q., Chen, A.R. and Dai, L. (2012), "Experimental investigation of movable hybrid GFRP and concrete bridge deck", *Constr. Build. Mater.*, **26**(1), 49-64.
Hillman, J.R. and Murray, T.M. (1990), "Innovative floor systems for steel framed buildings", *Proceedings of Mixed Structure, including New Materials*, Zurich, Switzerland.
International federation for structural concrete (CEB-FIP) (2010), FIP Bulletin 55: Model Code 2010, First complete draft-Volume 1, Switzerland.
Jeong, J., Lee, Y.H., Park, Y.K. and Hwang, Y.K. (2007), "Field and laboratory performance of a rectangular shaped glass fiber reinforced polymer deck", *Compos. Struct.*, **81**(4), 622-628.
Keller, T. and Gürtler, H. (2005), "Quasi-static and fatigue performance of a cellular FRP bridge deck adhesively bonded to steel girders", *Compos. Struct.*, **70**(4), 484-496.
Keller, T., Schaumann, E. and Vallée, T. (2007), "Flexural behavior of a hybrid FRP and lightweight concrete sandwich bridge deck", *Compos. Part A*, **38**(3), 879-889.

Kitane, Y., Aref, A.J. and Lee, G.C. (2004), "Static and fatigue testing of hybrid fiber-reinforced polymer-concrete bridge superstructure", *J. Compos. Construct.*, **8**(2), 182-190.
Klowak, C., Memon, A. and Mufti, A. (2006), "Static and fatigue investigation of second generation steel-free bridge decks",*Cement Concrete Comp.*, **28**(10), 890-897.
Kumar, P., Chandrashekhara, K. and Nanni, A. (2004), "Structural performance of a FRP bridge deck", *Construct. Build. Mater.*, **18**(1), 35-47.
Lee, J., Kim, Y., Jung, J. and John, K. (2007), "Experimental characterization of a pultruded GFRP bridge deck for light-weight vehicles", *Compos. Struct.*, **80**(1), 141-151.
Liu, Z., Cousins, T.E., Lesko, J.J. and Sotelino, E.D. (2008), "Design recommendations for a FRP bridge deck supported on steel superstructure", *J. Compos. Construct.*, **12**(6), 660-668.
Oh, B.H. (1986), "Fatigue analysis of plain concrete in flexure", *J. Struct. Eng. ASCE*, **112**(2), 273-288.
Park, Y.K., Hwang, Y.K., Lee, Y.H. and Kim, S.M. (2007), "Performance verification of a new pultruded GFRP bridge deck-to-girder connection system", *Compos. Struct.*, **81**(1),114-124.
Ringelstetter, T.E., Bank, L.C., Oliva, M.G., Russell, J.S., Matta, F. and Nanni A. (2006), "Cost-effective structural stay-in-place formwork system of fiber – Reinforced polymer for accelerated and durable bridge deck construction", *Transport. Res. Rec.: J. Transport. Res. Board*, **1976**, 183-189.
Schaumann, E., Vallée, T. and Keller, T. (2008), "Direct load transmission in hybrid FRP and lightweight concrete sandwich bridge deck", *Compos. Part A*, **39**(3), 478-487.
Sendeckyj, G.P. (1990) "Life prediction for resin-matrix composite materials", Fatigue of composite materials, Elsevier Science, Amsterdam, Netherlands.
Van Erp, G., Cattell, C. and Ayers, S. (2005), "The Australian approach to composites in civil engineering". *Reinf. Plast.*, **49**(6), 20-26.
Wan, B., Rizos, D.C., Petrou, M.F. and Harries, K.A. (2005), "Computer simulations and parametric studies of GFRP bridge deck systems", *Compos. Struct.*, **69**(1),103-115.
Zi, G., Kim, B.M. and Hwang, Y.K. (2008), "An experimental study on static behavior of a GFRP bridge deck filled with a polyurethane foam", *Compos. Struct*, **82**(2), 257-268.

BU